When Left Does Not Seem Right: Epigenetic and Bioelectric Differences Between Left- and Right-Sided Breast Cancer

Sofia Masuelli
IHEM: Instituto de Histologia y Embriologia Mendoza Dr Mario H Burgos
Sebastián Real
IHEM: Instituto de Histologia y Embriologia Mendoza Dr Mario H Burgos
Emanuel Campoy
IHEM: Instituto de Histologia y Embriologia Mendoza Dr Mario H Burgos
Maria Teresita Branham
IHEM: Instituto de Histologia y Embriologia Mendoza Dr Mario H Burgos
Marzese Diego Matías
Cancer Epigenetics Laboratory, Health Research Institute of the Balearic Islands (IdISBa), Palma, Spain
Matthew Salomon
USC Keck School of Medicine: University of Southern California Keck School of Medicine
Gerardo De Blas
IHEM: Instituto de Histologia y Embriologia Mendoza Dr Mario H Burgos
Rodolfo Arias
IHEM: Instituto de Histologia y Embriologia Mendoza Dr Mario H Burgos
Michael Levin
Tufts University
Maria Roqué Moreno (mroque@mendoza-conicet.gob.ar)
IHEM: Instituto de Histologia y Embriologia Mendoza Dr Mario H Burgos https://orcid.org/0000-0002-9564-1032

Research Article

Keywords: asymmetry, laterality, left, right, cancer

Posted Date: November 8th, 2021

DOI: https://doi.org/10.21203/rs.3.rs-1020823/v1

Version of Record: A version of this preprint was published at Molecular Medicine on February 5th, 2022. See the published version at https://doi.org/10.1186/s10020-022-00440-5.

When Left does not seem Right: Epigenetic and Bioelectric differences between Left- and Right-sided Breast Cancer

Masuelli Sofía[1,2], Real Sebastián[1, 2], Campoy Emanuel[1, 2], Branham María Teresita[1,3], Marzese Diego Matías[4], Salomon Matthew[5], De Blas Gerardo[1, 2], Arias Rodolfo[1], Levin Michael[6] and Roqué María[*1,7].

[1]National Council of Scientific and Technological Research (IHEM-CONICET), PC:5500, Mendoza, Argentina

[2]Medical School, National University of Cuyo, PC:5500, Mendoza, Argentina

[3]Medical School, Mendoza University, PC:5500, Mendoza, Argentina

[4] Cancer Epigenetics Laboratory, Health Research Institute of the Balearic Islands (IdISBa), Palma, Spain

[5]Department of Medicine, Keck School of Medicine, University of Southern California, Los Angeles, CA 90007, California, United States of America

[6] Allen Discovery Center at Tufts University, Medford, Massachusetts, MA 02115, United States of America

[7]Exact Science Faculty, National University of Cuyo, PC:5500, Mendoza, Argentina

[*]Corresponding author and lead contact:

María Roqué, mroque@mendoza-conicet.gob.ar, +542614054843

Running title: consistent laterality of breast cancer

ABSTRACT

Background: During embryogenesis, lateral symmetry is broken giving rise to Left/Right (L/R) breast tissues with distinct identity. L/R-sided breast tumors exhibit consistently-biased incidence, gene expression, and DNA methylation. We postulate that a differential L/R tumor-microenvironment crosstalk generates different tumorigenesis mechanisms. Methods: We performed in-silico analyses on breast tumors of public datasets, developed xenografted tumors, and conditioned MDA-MB-231 cells with L/R mammary extracts. Results: We found L/R differential DNA methylation involved in embryogenic and neuron-like functions. Focusing on ion-channels, we discovered significant L/R epigenetic and bioelectric differences. Specifically, L-sided cells presented increased methylation of hyperpolarizing ion channel genes and increased Ca^{2+} concentration and depolarized membrane potential, compared to R-ones. Functional consequences were associated with increased proliferation in left tumors, assessed by KI67 expression and mitotic count. Conclusions: Our findings reveal considerable L/R asymmetry in cancer processes, and suggest specific L/R epigenetic and bioelectric differences as future targets for cancer therapeutic approaches in the breast and many other paired organs.

Keywords: asymmetry, laterality, left, right, cancer

BACKGROUND

Some organs, such as the heart or viscera are asymmetric: their structures to the left and right of the body mid-plane are consistently different in all normal individuals [1]. Most other tissues are often believed to be symmetrical. However, major knowledge gaps exist about the degree to which paired structures could exhibit not only the fluctuating asymmetry of developmental noise but consistently biased asymmetry that might impact structure and function. Despite the general assumption that mammary glands are mere copies of one another, each gland has its

own identity and presents left-right (L/R) asymmetries. During embryogenesis of bilateral organisms, lateral symmetry is broken at very early stages in a programmed and consistent way [2][3][4]. The establishment of the L/R axis is the start of a regulated patterning, through which asymmetric sides arise at morphological, functional and molecular levels [5][6][1]. Alterations in laterality decisions during development give rise in humans not only to a reversed laterality (*situs inversus*) but also to an increased susceptibility to other diseases [7]. In particular, tumors in bilateral organs such as breast, colon, kidney or lung, show subtle but significant differences at morphological, genetic, molecular and incidence levels [8][9]. Research data from our group and others (of diverse disciplines such as embryogenesis, development, molecular oncology, or cellular biology), have proposed that the asymmetric tumor microenvironment of bilateral organs could be part of the explanation for the L/R differences in cancer [10] [8][3][4][11][12].

Tumor cells sense the environment and fire, in consequence, internal signals. By this, the tumor transcriptome differs from the surrounding normal tissue and acquires specific features. The gene expression shift that the tumor applies to face the environmental challenges depends on the surrounding tissue signals, especially during the initial tumorigenesis stages. Thus, it can be said that the microenvironment contributes to the decision-making strategy of a tumor to reach the cancer hallmarks [13]. In this context, epigenetics and bioelectricity have a crucial role since both constitute vehicles by which external signals reach and modulate the transcriptome in an experience-dependent and dynamic way.

Epigenetic modifications highly influence the biology of cancer. A key feature of cancer cells is to respond rapidly to environmental challenges, and this is mainly attributed to the dynamic plasticity of the epigenetic mechanisms. Epigenetic regulators have both writing and erasing capacities, so are therefore able to maintain a flexible transcriptome which is crucial for tumor development and survival (reviewed in [14]). In addition, epigenomes are also defined as the

bridges between the environment and the phenotype (or transcriptome)[15]. Being more dynamic and reversible than the genome, epigenomic variations can rapidly provoke a transcriptomic shift without changing the genomic sequence. DNA methylation, the most studied epigenetic modification, presents a specific signature associated with some cancer types, suggesting a distinct interplay between the tumor epigenome and the surrounding tissue. Based on this, specific aberrant DNA methylation patterns have been proposed as predictive and prognostic markers for several cancer types [16][17][18][19]. Specifically, in breast cancer, previous work of our group has identified that the DNA methylation profiles of tumor suppressor genes correlate with prognosis index [20][21], with tumor subtypes [22], migration and metastasis capacity [23] [24], benign mammary lesions [25], and, more relevant for the topic of this study, with the laterality of the tumors [10]. In summary, tumor epigenome is influenceable by the microenvironment and can be associated with differential tumor behaviors.

Bioelectric gradients are considered epigenetic mediators in a broad sense of the word since they can modify the transcriptome following environmental signals [26][27][28]. The flow of ions (inside the tumor and between the tumor and the microenvironment) enables the transmission of membrane potential patterns, which are maintained as information for survival decisions in response to external challenges [29][30]. Like epigenetics, bioelectric control is reprogrammable, rapid and dynamic, and is driven by physiological states that are not 1:1 mapped to specific genes [30]. Bioelectric states are acquired by ion flux through channels and pumps in the membrane and are transmitted to neighboring cells via gap-junctions. The current flux produces changes in membrane potentials, which in turn generate downstream signaling to regulate different cellular processes, e.g. proliferation [31], migration, differentiation, or gene expression. Therefore, it is accepted that cells of the same tissue share similar bioelectric states, which is maintained as non-genetic information. This is also applicable to the L/R sides of bilaterian bodies, where metabolic [32], epigenetic, bioelectric, and gene-expression differences

[33] have been reported. Just to highlight an example, L/R bioelectric differences have been observed in Xenopus and chicken embryos, finding consistent voltage and ion transporter asymmetries as early as the 2nd cell division [34]. These bioelectric differences subsequently regulate asymmetric gene expression to control the sidedness of asymmetric organs and paired structures such as eyes and neural crest derivatives [35].

Differences in L/R bilateral tumors have been reported for several cancer types, like breast [36],[37], colon [9],[38],[39], kidney [40],[41], brain [42], ovary [43], and eye [44]. Particularly in breast tumors, in addition to the largely known increased L-side incidence [45] [46], interesting differences in gene expression [8] [33], gland microbiota [47], mitochondria distribution [48] and methylation profiles [10] have been reported. It is reasonable to postulate that L/R adult glands conserve memories of their asymmetric embryogenic development, maintaining different L/R bioelectric patterns. These patterns are, in part, constituted by "attractors" (such as morphogens, neurotransmitters, small molecules) that trigger downstream different signaling pathways and change transcription regulation [30].

In this work, we hypothesize that tumorigenic breast processes face environmental challenges that differ between L/R sides, establishing a side-dependent tumor-microenvironment crosstalk reflected in bioelectric and epigenetic differences. A serendipitous finding during our previous research gave rise to the present work, when we discovered that DNA methylation patterns of female patient's breast tumors clustered in two groups based on whether they were located on the L or R gland [10]. This striking observation opened the questions of whether these L/R differences were reproducible in an in-silico, in-vivo and/or in-vitro model, and if functional differences were associated with these epigenetic profiles. In this work, we developed in-silico, in-vivo and in-vitro approaches to address these questions.

METHODS

Collection of in-silico data from public datasets.

For gene methylation analyses, *Illumina Infinium Human Methylation-450* information was obtained from breast cancer TCGA dataset, available in the public platform cBioportal for Cancer Genomics (https://www.cbioportal.org/, repository Firehose Legacy of the Broad Institute). The DNA methylation data is found in the repositories as beta values, which are continuous ratios between 0 and 1, indicating the intensities between methylated and unmethylated alleles (0 being unmethylated and 1 fully methylated). For laterality data, clinical datasets were also retrieved from the same platform. We used 530 primary breast tumors for which DNA methylation data of ~16,000 genes plus anatomical location (L/R gland) was available. After curating the information, we calculated the L/R DNA methylation mean for each genomic region and ranked their absolute differences (called from now on differential methylation, DM) (note: for all experiments, differences are calculated as *left minus right).*

To find the cellular and molecular functions in which the most differentially methylated genes were involved, we performed gene enrichment analyses with the public tools Metascape (https://metascape.org,RRID:SCR_016620) and EnrichR (https://maayanlab.cloud/Enrichr/enrich, RRID:SCR_001575). For Metascape tool, the enrichment analyses were set as: minimum overlap=3 and p value cutoff=0.001, with Gene priorization by Evidence Countins (GPEC). To establish the potential functional consequences of the proximal (up to 2.5kb up and downstream) as well as the distal (up to 1Mb up and downstream) genomic context of the differential methylated CpGs, GREAT analyses were performed (Genomic Regions Enrichment of Annotations Tool v4.0.0**)** [49]. We used the basal plus extension configuration as a background setup “whole genome”, as recently shown[50].

For gene expression analyses for selected genes of interest, *Illumina HiSeq 2000 RNA Sequencing platform* of the University of North Carolina was obtained from breast cancer TCGA dataset, available in the UCSC (University of California Santa Cruz) Xena Functional Genomics explorer

(http://xena.ucsc.edu/, RRID:SCR_018938). The RNA-Seq data are shown in the dataset as normalized log2 (x+ 1) values and indicate an estimated gene expression level.

Xenografts generation

The highly immunosuppressed Nod Scid Gamma mice (NOD.Cg-PrkdcscidIl2rgtm1Wjl/SzJ, NSG) (RRID:IMSR_JAX:005557) were obtained from Jackson Laboratory and were housed in a pathogen-free condition throughout the experimental duration. All procedures were performed following the consideration of animal welfare and were approved by the Institutional Committee for Care and Procedures of Laboratory Animals (CICUAL in spanish) of the National University of Cuyo, Mendoza, Argentina. To perform the xenograft experiment, six-week-old female NSG (20 grams) mice were anesthetized with isofluorane 4% in O_2, and injected with 1×10^6 MDA-MB-231 cells (suspended in physiologic solution) in the 4th L/R breast glands. Mice were closely monitored, and tumor size was measured weekly. Five weeks after cell inoculation, the mice were sacrificed in a CO_2 camera, and tumors were excised. Part of the tumors was set apart and frozen at -80°C for further DNA and RNA extractions (called tumors passage 0). The remaining parts were reimplanted in small pieces in 3 NSG mice, maintaining laterality (called tumors passage 1). The complete procedures were repeated in 3 more NSG mice to generate tumors passage 2.

Nucleic acid extraction

DNA was extracted from xenograft tumor tissues and from MDA-MB-231 cells, using PureLink® Genomic DNA Kits, Mammalian Tissue and Mouse/Rat Tail Lysate (Catalog Numbers K1820-02, Invitrogen), following manufacturer's protocol. RNA was extracted from MDA-MB-231 cells using a Trizol based protocol (TRIzol® Reagent (Life technologies, Catalog Numers 15596-026).

DNA Methylation analyses by MS-MLPA and RRBS

To assess the methylation status of 50 CpG sites located on 40 genes, the MS-MLPA kits ME001 and ME002 (Catalog Numbers ME001-025R, ME002-025R) were used. The MS-MLPA assays were performed basically according to manufacturer's recommendations (MRC-Holland, Amsterdam, The Netherlands, www.mrc-holland.com)[51], introducing subtle modifications (i.e., extended restriction enzyme incubation time, separated ligation and digestion steps), to avoid background signals[20]. The fluorescent-labeled PCR products were separated by capillary electrophoresis (3500 Genetic Analyzer for Fragment Analysis, Applied Biosystems) and analyzed by GeneMarker v1.75 software (RRID:SCR_015661). A cutoff of 8% fluorescence signal was established to consider the site significantly methylated.

To assess an extended methylation analysis involving most of the genome CpG sites, a reduced restricted bisulfite sequencing (RRBS) assay was performed with the technical and bioinformatic assessment of the Genomic Unit–Consortium CATG-National Institute of Agricultural Technology (INTA) in Buenos Aires, Argentina. For this, 3 left and respective right xenograft passage 1 tumors were selected. The experimental steps consisted on: preparation of the libraries with Diagenode's Premium RRBS kit (Diagenode, Cat. No. C02030032), sodium bisulfite conversion of the DNA samples and PCR amplification and sequencing of the generated fragments on an Illumina NextSeq 550 equipment. Quality control of sequencing reads was performed using FastQC® (Babraham Bioinformatics®, RRID:SCR_014583). Adapter removal was done using Trim Galore® version 0.4.1 (Babraham Bioinformatics®, RRID:SCR_011847). Reads were then aligned to the reference genome GRCh38 using Bismark v0.22.1.® (Babraham Bioinformatics®, RRID:SCR_005604), followed by methylation calling using the corresponding bismark functionality. The comparison between the RRBS data sets was carried out using methylKit® (Bioconductor®, RRID:SCR_005177), with the GRCh38 refGene and CpG island annotation from UCSC (University of California Santa Cruz, RRID:SCR_006553) genome browser. Bioinformatic

filters were applied on the raw results, to select only human sequences aligned with the human refence genome GRCh38, discarding possible mice or other organism's genomic interference. After methylation calling, and difference calling with Bioconductor 3.9, L/R significant DM with more than 10% difference were found in 1,239 sites (q value <1x10-8). We selected this cut-off to consider differentially methylated CpGs (DMG).

Cell culture.

Human breast cancer cell line MDA-MB-231 (ATCC, RRID:CVCL_0062) was kindly provided by Dr. Matias Sanchez (IMBECU Institute, Mendoza, Argentina) and passages 20-30 were used for this work. The cells were routinely tested for mycoplasma contamination. In general, cells were cultured in DMEM medium (Gibco by Life Technologies, Grand Island, NY, USA, # 112800-058) supplemented with 10% fetal bovine serum (Internegocios S.A, Mercedes, BA, Argentina), 100 U/mL of penicillin and 100 μg/mL streptomycin (Gibco by Life Technologies, Grand Island, NY, USA, #1796440), at 37°C in a humidified atmosphere containing 5% CO_2. For the extract-conditioned cultures, fetal bovine serum was reduced to 1%.

L/R extract preparation and conditioned cell culture.

Healthy L/R breast glands were obtained from plastic surgeries, provided by Dr. Cataneo from the Clinic of Plastic Surgery of Mendoza, after patients signed an informed consent previously approved by the Ethics Committee of the Medical School of the National University of Cuyo. Tissues were first disaggregated with a scalpel and the pieces were suspended in 25 ml of DMEM medium with Penicillin/Streptomycin 1% and incubated in a shaker for 24hr at 37°C. Next, samples were centrifuged to remove the solid fat and the remaining suspension was filtered with cell strainers of first, 100μm and afterwards 40μm, to eliminate residual tissue parts. The obtained liquid-phase extracts were L/R labeled and stored for further experiments at -20°C.

MDA-MB-231 were conditioned with a cocktail consistent of 49% DMEM with Penicillin/Streptomycin, 1% Serum Fetal Bovine and 50% left or right liquid-phase extract.

Monitoring changes in Ca2+ concentration and $\Delta\psi_p$.

Cells were cultured on 30mm glass coverslips for performing Ca2+ imaging. Coverslips with cells attached were mounted in a chamber and incubated at 37°C and protected from the light for 30 min in a culture medium containing 3 µM Fluo3-AM (Invitrogen, Cat# F1242). After incubation, cells were washed 2 times with PBS 1X and bathed in DMEM medium supplemented with 10% fetal bovine serum , 100 U/mL of penicillin, and 100 µg/mL streptomycin for 5 min before Ca2+ measurements were made.

After washing to remove the unincorporated dye, the coverslips were mounted in a recording chamber placed on a temperature-regulated platform (37°C) of an inverted Olympus FV 1000 confocal microscope (Olympus Corporation, Tokyo, Japan). Images were collected using the Fluoview FV-1000 software and an Olympus 20X lens (UPlanSApo 20X/0.75). Fluo 3 fluorescence was detected using the filter cube U-MWB2 (excitation BP 460-490 nm and emission LP 520 nm). Images were analyzed with Microsoft Excel and Image J (National Institutes of Health, USA, RRID:SCR_003070).

For $\Delta\psi_p$ measurements, $10x10^4$ MDA-MB-231 cells were plated and conditioned with L/R extracts for 5 days as described above, and then incubated for 30min with 1µM $DiBAC_4(3)$ (Bis-1,3-Dibutylbarbituric AcidTrimethine Oxonol, a fluorescent probe for membrane potential determination) (Invitrogen by Thermofisher Scientific, Cat. No. B438) at 37°C and 5% CO_2. Afterwards, cells were trypsinized and fluorescence was measured by flow cytometry (FACSARIA-III, BD-Biosciences®) with a BP 530/30 emission filter. Results were analyzed using FlowJo v X.0.7® software (RRID:SCR_008520).

Local Breast cancer female patient mitotic index data

From a previous work of our group [10], we counted with a database of 95 breast cancer female patients (mean age 54, range 31-86) who had previously signed an informed consent approved by the Ethics Committee of the Medical School of the National University of Cuyo, Mendoza, Argentina. The database included information of the tumor mitotic index provided by the same anatomo-pathologist. In brief, at least 10 different areas had been counted and cells in metaphase, anaphase or telophase were considered in mitosis as indicated in [52]. We dichotomized the data as *low mitotic index* with a mean of up to 19 mitotic cells/area and *high mitotic index* with a mean of 20 or more mitotic cells/area.

Statistical analyses.

Differences between 2 proportions of *hyper/depolarizing* ICH were calculated as Odds Ratios (OR), with the corresponding 95% CI. To compare means and medians of fluorescent-probes concentrations, unpaired T-test was applied with Welch's corrections when variance was not equal among L/R data. L/R ratio differences were analyzed by One sample T-test with hypothetical Right value=1 (assigning the values of Right as reference). When more than two groups were compared, one or two-way Anova test were applied (with Dunnet post-test). Finally, Fisher's exact test was used to compare categorical data. *P* values below 0.05 were considered as statistically significant.

RESULTS

DNA Methylation Differences

In-silico L/R DNA Methylation differences in breast tumors

The methylation profile of ~16000 genomic regions were analyzed in 782 primary breast carcinomas (394 L and 388 R). We calculated the L/R DNA methylation mean for each genomic region and ranked their absolute differences (called from now on differential methylation, DM), which ranged between 10^{-7} and 5 %, with a median value = 0.03%. We decided to focus on the top genes with >1% difference. Gene Enrichment analyses performed on the selected genes by Metascape (https://metascape.org) revealed that the main pathways in which they were involved were related to *regulation of ion transport* (GO:0043269), *trans-synaptic signaling* (GO:0099537), and *embryonic morphogenesis* (GO:0043598) (Figure 1A). By the tool EnrichR (https://maayanlab.cloud/Enrichr/enrich), also *embryonic digestive tract development* (GO:0048566)*, chemical synaptic transmission (GO: 0007268), calcium ion transport (GO: 0006816),* and *positive regulation of ion transport* (GO:0043270) appeared as significantly involved pathways (adjusted p values <0.05).

In-vivo L/R DNA methylation differences in an animal model.

To study whether the L/R DM was reproducible in an animal model, we generated synchronic L/R breast tumors in Nod-Scid-Gamma (NSG) immune depressed mice by inoculating the human breast cancer cell line MDA-MB-231 simultaneously in both 4^{th} mammary glands. After generating three sequential passages (called P_0, P_1, and P_2), the tumors were first analyzed in a reduced number of CpG sites by Methyl-Specific-MLPA (50 CpG sites located on 40 tumor suppressor genes). The three passages showed subtle L/R differences in several genes, and we chose P_1 as the passage with the major DM. In 15 CpG sites of 11 genes (*RASSF1A, ESR, IGSF4, CDH13, MGMT, TP73, WT1, MSH6, PAX6, GATA5,* and *RARB*) the L/R DM per site were from -6.8% to 11.17%. These observations were considered only useful for choosing a tumor passage to scale up experimentally and perform a whole genome methylation analysis.

In the light of this, DNA of the three P_1 L/R paired xenograft tumors were selected for Reduced Restricted Bisulfite Sequencing (RRBS) assays. After establishing an arbitrary cut-off of 10% DM, (see Methods for more details), we decided to discard inflammation-response genes, since they are known to increase their expression after surgical manipulation [53]. On the remaining genes, gene enrichment analyses performed by Metascape revealed *cellular* (GO:0032989) and *tissue morphogenesis* (GO:0048729), several *developmental pathways* (e.g., GO:0001655; GO:0021700; GO:0021675), *morphogenesis of a branching structures* (GO:0001763) and *chemical synaptic transmission* (GO:0007268) as the main GO biological processes (Figure 1B). Furthermore, Genomic Region Enrichment Analyses (GREAT) [49] showed that the overall differences were mainly involved in the GO biological processes *embryonic camera-type eye development* (GO:0031076), *epidermis development* (GO:0008544), *mammary gland development* (GO:0030879), and *regulation of neuronal synaptic plasticity* (GO:0048168). So very interestingly, the generated animal model revealed biological processes following what we previously had found in human in-silico data of breast tumors, indicating that L/R differences were consistently associated with **embryogenic** and **neuronal** features.

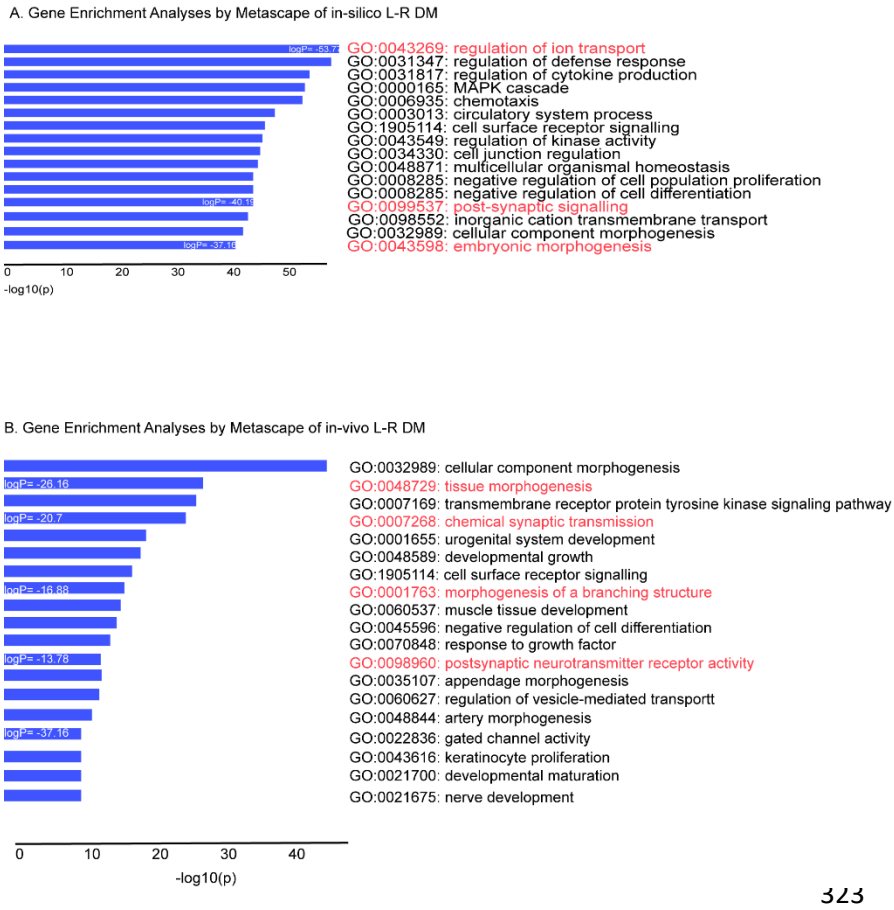

Figure 1. L-R Gene enriched pathways of L-R differential methylated regions. A. DNA regions with more than 1% DM between L-R primary breast tumors from TCGA public dataset were analyzed by Metascape for enriched GO Biological processes (p value cut-off 0.001). Ion/neural and embryonic pathways are highlighted in red. **B.** DNA regions with more than 10% DM between 6 L-R xenograft tumors were analyzed by Metascape for enriched GO Biological processes (p value cut-off 0.001). Neuronal and morphogenic involved processes are highlighted in red.

Focus on ion-channel genes among the in-silico and in-vivo L/R methylation differences.

The role of electrochemical gradients in neurons is well known. However, an increasing amount of literature is revealing the role of electrochemical gradients in the regulation of diverse functions of *non*-neuronal cells, including morphogenesis of numerous embryonic and adult structures[54],[55],[56]. Consistently, the GO term *ion transport* had appeared among the in-silico main enriched pathways. We therefore decided to search whether ion-channel genes were included in our DM lists.

We found 33 ICH genes matches (using as refrerence the Human Gene Nomenclature Committee (HGNC) ion channel list (https://www.genenames.org/data/genegroup/#!/group/177) among the in-vivo DM and 77 ICH genes in the in-silico data (Table 1). Positive DM was indicating increased DNA methylation in L-sided tumors ("more methylated left" -MML- in Table 1); and negative DNA methylation differences indicated "more methylated right" -MMR-. Very notably, we noticed a tendency for increased percentage of *hyperpolarizing* channels among the MML genes, as compared to MMR ones (66.6% vs 54.8%, OR=2, 95%CI:0.46-8.5 in the in-vivo experiment; and 54.5% vs 49%, OR=1.24, 95%CI:0.46-3.35 in the in-silico approach) (Figure 2). Even though these differences did not reach statistical significance, the repeated tendency in both approaches suggested a possible non-stochastic pattern. Furthermore, this pattern did not appear gene-specific (as can be inferred from Table 1). So we reasoned that it could be possible that the L/R breast tumor differences occurred at bioelectric levels, preserving a consistent voltage change direction but in a non-specific gene manner.

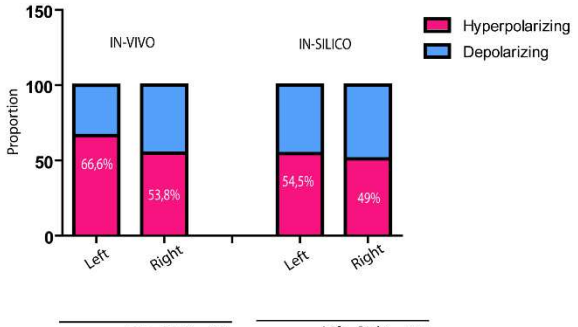

	Left	Right	OR
Hyperpol	14	7	
Depol	6	6	2 (0,4-8,5)
Total	20	13	
%	66,6	53,8	

	Left	Right	OR
Hyperpol	12	27	
Depol	10	28	1,24 (0,4-3,3)
Total	22	55	
%	54,5	49	

Figure 2. L-R Comparison of methylated hyper vs depolarizing ion channels. Data from in-vivo and in-silico analyses. Tendency shows in both approaches L-sided tumors with increased proportion of

methylation in hyperpolarizing channels, as compared to R ones (66.6% vs 53.8% in-vivo and 54.5% vs 49% in-silico).

Taken together so far, L/R epithelial carcinomas presented methylation differences in genes involved in embryogenic and neuronal processes, showing a striking pattern in ion channel genes, suggesting increased DNA methylation of hyperpolarizing genes on L-sided tumors. Inferring from our xenograft experiments, we could discard that these differences were original of the tissue where the tumor started (since mice-genomic interferences had been filtered), which allowed us to adventure that they were acquired during the tumor progression.

To establish the environmental role in acquiring bioelectric and DNA methylation differences, we further continued with in-vitro studies.

(Insert Table 1)

Bioelectric Differences

In-vitro L/R Ca2+ differences in conditioned cell culture.

To establish how (or if) the mammary gland microenvironments contributed to the L/R voltage differences, we set up an in-vitro model where cellular extracts of healthy L/R human mammary tissue were used to induce changes in cultured cells. From surgical reductions of healthy L/R mammary glands, we included samples from four women (median age 34) in this study. Paired L/R cellular extracts from one female donor (W1) were first used to treat MDA-MB-231 breast cancer cells for five days, afterward measure Ca2+ concentration with a calcium fluorophore by confocal microscopy and quantify the concentration. We counted between 50-100 cells for each treatment and confirmed that the L/R W1 extracts had a different effect on cells, showing an increased Ca2+ concentration in the left-treated cells (Figure 3) (unpaired T-test with Welch's correction, $p<0.003$). With this, we confirmed that the developed in-vitro model was sensitive

and reproducible to test the effect of L/R extracts on cellular electricity. Furthermore, the generated difference in Ca2+ concentration suggested that L-treated cells had relatively depolarized their plasma membrane. To further explore this, we advanced with membrane potential analyzes.

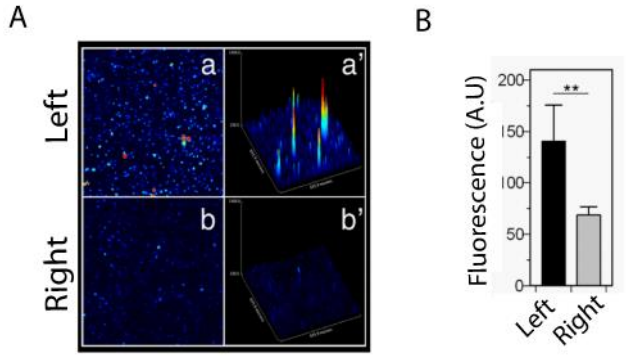

Figure 3. L-R Ca2+ concentration comparison. MDA-MB-231 cells treated with L-R normal breast extracts from donor W1 and measurement of intracellular calcium concentration with Fluo3 AM. **A**. Representative calcium fluorescence in two-dimensional (a and b) and three-dimensional images -surface plot- (a' and b'). Pseudo-color from black to red represents low to high intracellular calcium concentration, respectively. **B.** Fluorescence quantification reveals a significant increment of intracellular calcium concentration in the L-treated cells. Values represent the mean ± SEM from 3 independent experiments, 50-100 cells were analyzed per experiment. (unpaired T-test with Welch's correction, $p<0.003$).A.U: artificial units

In-vitro L/R $\Delta\psi_p$ differences in conditioned cell culture.

The voltage-sensitive dye specific for plasma membrane potential ($\Delta\psi_p$) Bis-(1,3-Dibutylbarbituric Acid) Trimethine Oxonol ($DiBAC_4(3)$) was used to measure the effect of L/R mammary tissue extracts on MDA-MB-231. The dye (negatively charged) accumulates into depolarized cells. It has been previously established by others that this method is reliable for

bioelectric studies in non-neuronal cancer cells which are known to be less polarized than normal cells [57].

The L/R extracts of three female donors (W2, W3, W4) were used to perform treatment replications. After five days of treatment, the $DiBAC_4(3)$ signal was measured by flow-cytometry. Interestingly, the L-treated cells displayed an increment in the fluorescence signal, indicating a less polarized state, in line with our previous assumption (L/R-fluorescence ratio, One-sample T-test with hypothetical R value=1, p=0.017, Figure 4A). This observation was consistent for each extract, although not all reached the statistical significance (W2: p=0.01, mean of difference 1.65; W3 and W4: L-treated NS increased tendency, three technical replicates, Figure 4B). When we mixed the L and R extracts in a pool and compared the effect, the generated difference was statistically significant (L/R-fluorescence ratio, One-sample T-test with hypothetical R value=1, p=0.03, mean of difference: 2.53, three technical replications, Figure 4B). With this, we confirmed that: *i*. the extracts had a differential bioelectric effect on the treated cells, *ii*. the effect was independent of the donor, and *iii*. the L-extracts generated a *depolarized* state as compared to R-extracts. Having confirmed this, we chose the pooled extracts for further studies to avoid possible donor-specific bias.

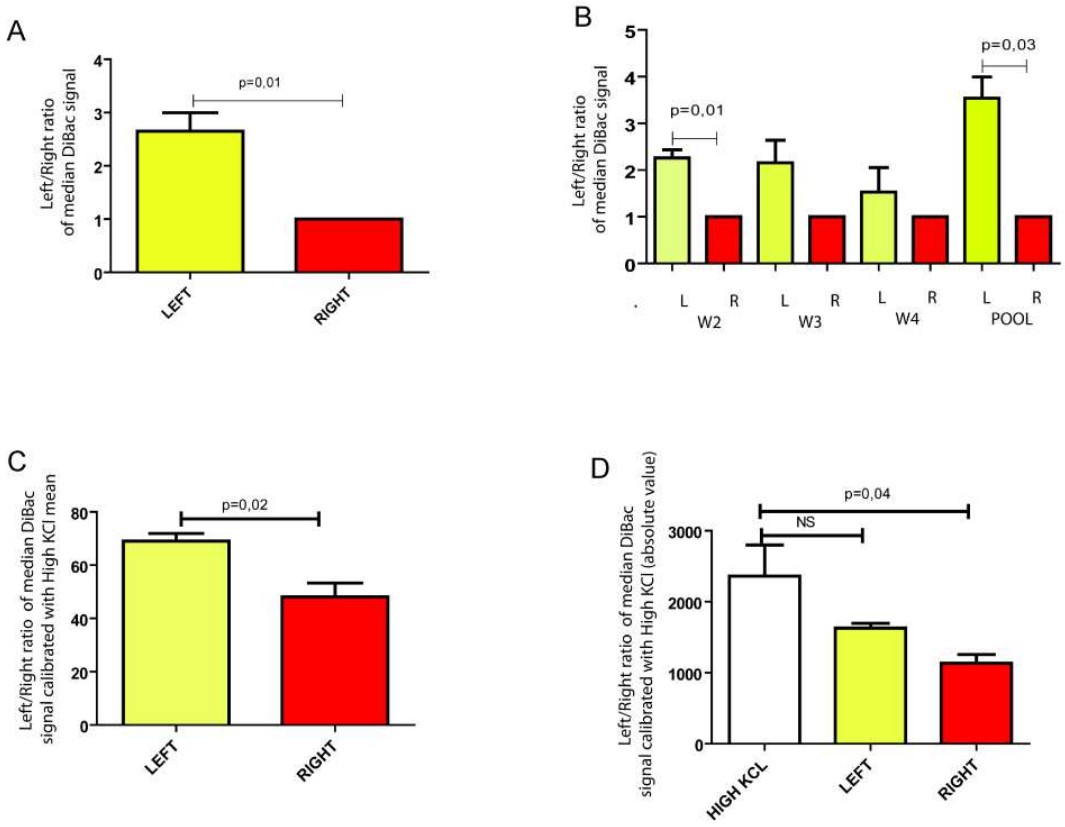

409

410 **Figure 4. L-R Membrane potential comparison in conditioned MDA-MB-231 cells**. **A**. The results are
411 expressed as the L median of $DiBAC_4(3)$ fluorescence relativized to R. N=3 experimental replications
412 (treatments with normal breast extracts W2, W3, W4). **B**. Individual analyses of the effect of L-R normal
413 breast tissue extracts on cells. The results are expressed as the L $DiBAC_4(3)$ fluorescence relativized to R.
414 The 3 extracts present increased $DiBAC_4(3)$ fluorescence in L-treated cells, although not all significant.
415 W2: p=0,01, mean of difference 1.65; W3 and W4: L-treated NS increased tendency; pool: p=0.03, mean
416 of difference: 2.53. One-sample T-test with hypothetical R value=1, for all experiments 3 technical
417 replicates were performed. **C.** L and R $DiBAC_4(3)$ fluorescence medians are expressed as percentages of
418 the median fluorescence of high-KCl treated cells. L-treated cells present higher fluorescence as compared
419 to the R ones (unpaired T test, p=0.02). **D.** Median fluorescence of high-KCl, L and R treated cells are
420 compared. Only the R-treated ones differ significantly from the completely depolarized (One-way Anova
421 + Dunnet post-test, p=0.0037).

422

Our following aim was to establish the magnitude of the L/R $\Delta\psi_p$ differences. For this, to normalize the potentials to a maximum depolarized state (100%), we treated cells with a depolarizing agent (65mM KCl, as suggested by Bonzanni et al. to depolarize MDA-MB-231 [57]). When expressing the $DiBAC_4(3)$ results as a percentage of the completely depolarized cells, we found that L-treated cells showed 69% (95% CI: 56.67-81.35) vs R-treated 48% (95% CI: 25.72-70.42), difference which was statistically significant (Unpaired T test, p=0.02, Figure 4C). Interestingly, however, no statistical difference was observed between L-treated cells and the KCl-treated ones, while R-treated cells did differ significantly (One-way Anova + Dunnet post-test, p=0.0037, Figure 4D). So we could conclude by this that the L-treated cells reached a similar depolarization as the maximum depolarized cells.

Epigenetic enzymes differences

In-silico L/R methyltransferase expression differences.

It has been well documented that epigenetics has a role in the adaptive regulation of gene expression. Specifically in neurons, in the dynamic expression of ion channels it has been reported that enzymes involved in DNA cytosine methylation have a crucial participation [58]. The process is catalyzed by DNA methyltransferases (DNMTs) and most commonly occurs at cytosines followed by a guanine, called CpG sites. DNMT3A is a de novo DNMT that methylates cytosines on unmethylated CpG sites, while DNMT1 is a maintenance DNMT that methylates cytosines on an unmethylated CpG with a methylated opposite strand. The inverse *de*-methylation process is regulated by the ten-eleven translocation (TET1, 2, and 3) family enzymes which oxidate the 5-methylcytosine to 5-hydroxymethylcytosine. We wondered whether these enzymes were differentially expressed in L/R mammary tumors.

From the TCGA-dataset of the Xena Functional Genomics Explorer (www. https://xenabrowser.net/), 1168 primary breast tumors (584 L and 584 R) were analyzed for *DNMT*s gene expression. L breast tumors presented increased expression of the 3 *DNMT* types (non-normally distributed data, Welch unpaired T-test, *DNMT1*: p=0.01; *DMT3a*: p=0.04; *DMT3b*: p=0.001) (Figure 5A). Instead, the demethylating enzymes *TET1, 2* and *3* did not present any difference associated with laterality in 1095 primary breast tumors (571 L and 524 R) (Figure 5B, non-normally distributed data, Welch unpaired T-test, $p>0.05$). As control, normal tissue was analyzed where none of the studied enzymes presented L/R differences. When comparing normal vs tumoral, all the enzymes had altered expression in tumors. The 3 *DNMT*s presented significantly increased expression (Unpaired T test, $p<0.0001$), *TET 1* and *2* decreased expression (Unpaired T test, $p<0.001$), and *TET3* increased expression (Unpaired T test, $p<0.001$), as compared to their side-respective normal tissue.

The observations suggest that, independently of the TET enzymes, the DNMTs are increased on the L-sided tumors, when compared to the R-ones. When deepening on the TET/DNMT relationship, it has been recently shown that TETs do compete with DNMTs in promoters of genes associated primarily to development and morphogenesis [59]. TETs act maintaining a hypomethylated state in these promoters, only in the absence of DNMTs. Based on these recent findings, one could ask whether increased methylation of hyperpolarizing ICH in L-tumors is due to enhanced DNMT activities, or/and if in R-tumors, with less DNMT activity, the TET enzymes are more actively demethylating the hyperpolarizing ICH.

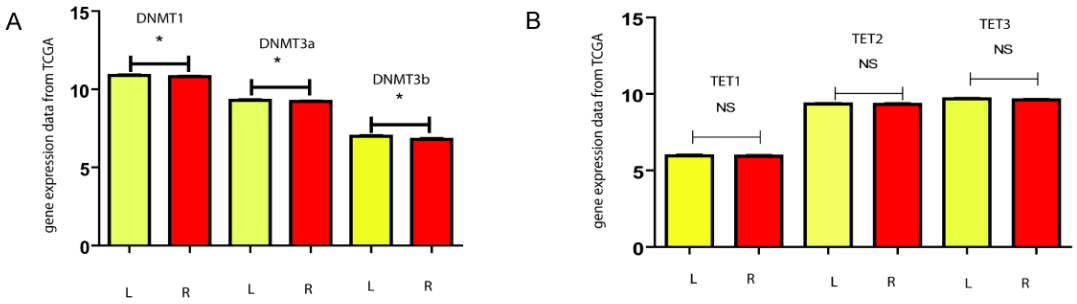

Figure 5. L-R Epigenetic modulators expression comparison. A. Gene expression data from 1100 TCGA L-R breast tumors. *DNMT*s present significant increased expression on L-sided tumors, as compared to the R ones. This is not accompanied by the *TET* genes (panel **B**), which do not differ in their expression regarding the side.

Proliferation differences

In-Silico L/R differences in KI67 expression.

A cell that needs to divide enters the cell cycle, and the regulation of the progression from one phase to the next one has been proposed to be coupled to environmental conditions so that this occurs only when it is necessary [60]. It is also known that the activity and expression of ion channels change during the cell cycle, and that Ca2+ concentration increases at the 3 cell cycle checkpoints and the membrane depolarizes between G_2 and Mitosis, as reviewed by Rosendo-Pineda et al [61]. We decided therefore to analyze whether the L/R tumors presented proliferation differences. The protein KI67 is widely used as a proliferation marker in different types of tumors. In-silico databases contain RNAseq values of *KI67*, obtained by Illumina HiSeq RNA Sequencing. We searched in breast in-silico datasets the expression of *KI67* and matched it with the tumoral laterality information. Of 1060 primary breast tumors of the TCGA breast cancer dataset (571 L and 489 R), we found a significant increment of *KI67* expression in L-sided tumors (Unpaired T-test, p=0.002, Figure 6A). Normal L/R breast tissue did not present

differences in *KI67* expression (Unpaired T-test, p>0.5). Both observations suggest a subtle increment of proliferation in L-sided tumors, as compared to the R-sided. This is consistent with our bioelectric findings since a depolarized state is necessary for cells to enter in mitosis.

In-vivo L/R mitotic index differences in female patient breast tumors

From our previous publication [10] we counted with a database of clinic-pathological information of 95 local female patients with breast cancer (mean age 54, range 31-86). Revising the data, we analyzed if side correlated with the tumoral mitotic count. To establish the mitotic index, 10 different areas had been counted and cells in metaphase, anaphase or telophase were considered in mitosis. We classified the tumors as *low mitotic index* with a mean of up to 19 mitotic cells/area and *high mitotic index* with a mean of 20 or more mitotic cells/area. In concordance with in-silico observations, we found significantly more tumors with high mitotic index on the L side (Fisher's exact Test, p=0.002, Figure 6B).

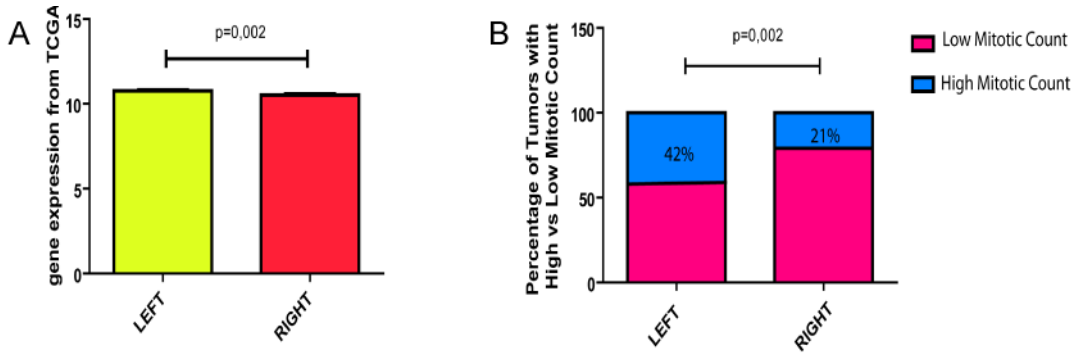

Figure 6. L-R Proliferation rate comparison by *KI67* and mitotic index. A. Comparison of L-R *KI67* expression in 1060 primary breast tumors from TCGA. L expression in significantly increased (Unpaired T-test, p=0.002). **B**. Proportion of 95 L-R IDC breast tumors from local female patients with high and low mitotic count (Fisher's exact Test, p=0.002).

DISCUSSION

Bioelectric fields are produced naturally in all living tissue. Not only excitable nerve and muscle cells, but all cell-collectives that are organized in a functional network generate bioelectric signals to communicate among each other. Long before neurons existed, evolution exploited bioelectric networks to regulate morphogenesis and behavior [62],[63]. When multicellular organisms appeared, the same efficient mechanism has been conserved for long-distance communication at different levels of the whole body. Bioelectric gradients are involved in embryogenic processes, such as eye development [64], brain shape[65], antero-posterior and L/R axes [34], and the control of appendage size and shape[66][67][68][69]. Endogenous bioelectric properties are seen to be critical due to numerous channelopathies in human and model systems, and there is an increasing realization that ion channels can also be oncogenes (reviewed in [68],[70],[71],[72],[73],[74] [75]. In 1938, Burr et al showed that tumorigenic processes in the mammary glands of mice were associated with disrupted bioelectric patterns in the chest [76]. Since 2000, when the tools to study bioelectricity increased significantly, many others have associated cancer with bioelectric alterations (reviewed in [77]) and discovered that the tumor microenvironment impacts on the bioelectric tumor pattern [78].

Epigenetics is also a key player in the interaction between cells and microenvironment. A rapid gene-expression shift is many times required to respond on time to the variable environment. We propose here a connection between epigenetics, environment, and bioelectric changes that the tumor cell senses, uses, and copes-with to shape a survival strategy.

In this work we have identified differences in methylation profiles and epigenetic regulators associated with distinct microenvironments (L/R), in addition to different bioelectric states and proliferation markers. We have found that L tumors present an increased expression of DNA

methylation enzymes, an increased proportion of methylated hyperpolarizing ICH genes, a more depolarized membrane potential, and an increment in proliferation markers or mitotic index. These results can complement related observations of other biological and medical fields. For example, in the clinic it is well known that breast cancer has a slightly lower incidence on right sides [46]. And others have explored that hyperpolarization decreases tumor incidence (Sundelacruz et al., 2009; Levin, 2012b; Chernet and Levin, 2014). Our results can connect both descriptions, by proposing that the more polarized state of R-sided tumors could explain the lower tumor incidence.

How this interplay between methylation, ion channels, voltage changes and proliferation occurs, in which order they are related or whether one is causative of the other are open questions for next studies. Are the methylation profiles responsible for the bioelectric differences? We did not find a strong inverse correlation between methylation and expression of the involved ICH genes in TCGA. The expression profiles of the ion channels which were found methylated did not reveal laterality differences in in-silico data. However, we think that this is explainable by the fact that the bioelectric differences are not gene-specific. So, probably it is not possible to establish a fixed panel of ion channel genes to study L/R differences. It is also possible to think on an inverse relation between bioelectricity and DNA methylation, where the epigenetic profiles are not causative but instead are a consequence of the bioelectric alterations, as has been proposed previously by others in neurons[28][26] and development[27].

Our in-vitro model has shown to be a reliable experimental tool to electrochemically transdifferentiate cells with L/R extracts. Although it is generally accepted that experiments in culture do not recapitulate the complexity of the cellular surroundings, our model produced repeatable and consistent results in concordance with what was observed in-silico and in animals. This encourages to postulated it as an efficient study tool for this purpose. Again, many

questions remain. What components of the L/R extracts are producing different polarization in cultured cells? Morphogens? Small molecules? Neurotransmitters? Ions?

CONCLUSION

If further studies establish that general tumors on bilateral organs differ in their membrane potential, it could open new candidate therapeutic options by, for example, designing cocktails of channel openers/blockers, which are widely used in the clinic [29]. The promising perspective is that, as proposed in [79], the interference with (or restoration of) bioelectric communication among tumor cells should be able to suppress carcinogenesis. Our work has opened new focuses based on L/R epigenetic and bioelectric differences in breast cancer, which could serve as prove of principle for other bilateral cancers like kidney, lung, testis, ovary and brain.

LIST OF ABBREVIATIONS:

DMG: Differentially methylated genes
DNMTs: DNA methyltransferases
ICH: Ion Channel
L:Left
MS-MLPA: Methylation Specific-Multiplex Ligation-Dependent Probe Amplification
NSG: Nod Scid Gamma
$\Delta\psi_p$: Plasma membrane potential
R: Right
RRBS: Reduced Restricted Bisulfite Sequencing
TCGA: The Cancer Genome Atlas
TET: ten-eleven translocation

DECLARATIONS

Ethics approval and consent to participate

The tumor data used from our previous study on 95 breast cancer female patients[10] counted with signed informed consent approved by the Ethics Committee of the Medical School of the National University of Cuyo, Mendoza, Argentina.

All procedures performed on the Nod Scid Gamma mice (NOD.Cg-PrkdcscidIl2rgtm1Wjl/SzJ, NSG) followed the consideration of animal welfare and were approved by the Institutional Committee for Care and Procedures of Laboratory Animals (CICUAL in spanish) of the National University of Cuyo, Mendoza, Argentina.

Availability of data and materials

The datasets supporting the conclusions of this article are included within the article and are available in the cBioportal of Cancer Genomics (Cerami et al. 2012; Gao et al. 2013) (http://www.cbioportal.org/) and Xena Functional Genomics explorer (http://xena.ucsc.edu/, RRID:SCR_018938).

Competing interests

The authors declare that they have no competing interests

Funding

This work was partly performed with funds of the Argentine Institute of Cancer (INC), National Health Ministery, grant “Epigenetica y Lateralidad en el Cáncer de Mama” 2016-2018.

Authors' contributions

Conceptualization: SM, SR, EC, MTB, ML, MR; Supervision: MR; Methodology: SM, SR, GDB, RA; Investigation: SM and MR; Data curation and Formal analysis: DMM, MS and MR; Writing, Review and Editing: SM, SR, EC, MTB, DMM, SM, ML and MR; Visualization: EC and MR.

Acknowledgements

We thank Dr. C Acosta and Dr. C García Samartino for their contributions in the membrane potential assays and cytometry determinations, respectively.

FIGURE TITLE AND LEYENDS

Figure 1. L-R Gene enriched pathways of L-R differential methylated regions. A. DNA regions with more than 1.25% DM between L-R primary breast tumors from TCGA public dataset were analyzed by Metascape for enriched GO Biological processes (p value cut-off 0.001). Ion/neural pathways and morphogenesis are highlighted in red. B. DNA regions with more than 10% DM between 6 L-R xenograft tumors were analyzed by Metascape for enriched GO Biological processes (p value cut-off 0.001). Neuronal and morphogenic involved processes are highlighted in red.

Figure 2. L-R Comparison of methylated hyper vs depolarizing ion channels. Data from in-vivo and in-silico analyses. Tendency shows in both approaches L-sided tumors with increased proportion of methylation in hyperpolarizing channels, as compared to R ones (66% vs 54.8% in-vivo and 54.5% vs 49% in-silico).

Figure 3. L-R Ca2+ concentration comparison. MDA-MB-231 cells treated with L-R normal breast extracts from donor W1 and measurement of intracellular calcium concentration with Fluo3 AM. A. Representative calcium fluorescence in two-dimensional (a and b) and three-dimensional images -surface plot- (a' and b'). Pseudo-color from black to red represents low to high intracellular calcium concentration, respectively. B. Fluorescence quantification reveals a

significant increment of intracellular calcium concentration in the L-treated cells. Values represent the mean ± SEM from 3 independent experiments, 50-100 cells were analyzed per experiment. (unpaired T-test with Welch's correction, $p<0.003$).

Figure 4. L-R Membrane potential comparison in conditioned MDA-MB-231 cells. A. The results are expressed as the L median of DiBAC fluorescence relativized to R. N=3 experimental replications (treatments with normal breast extracts W2, W3, W4). B. Individual analyses of the effect of L-R normal breast tissue extracts on cells. The results are expressed as the L DiBAC fluorescence relativized to R. The 3 extracts present increased DiBAC fluorescence in L-treated cells, although not all significant. W2: p=0,01, mean of difference 1.65; W3 and W4: L-treated NS increased tendency; pool: p=0.03, mean of difference: 2.53. One-sample T-test with hypothetical R value=1, for all experiments 3 technical replicates were performed. C. L and R DiBAC fluorescence medians are expressed as percentages of the median fluorescence of high-KCl treated cells. L-treated cells present higher fluorescence as compared to the R ones (unpaired T test, p=0.02). D. Median fluorescence of high-KCl, L and R treated cells are compared. Only the R-treated ones differ significantly from the completely depolarized (One-way Anova + Dunnet post-test, p=0.0037).

Figure 5. L-R Epigenetic modulators expression comparison. A. Gene expression data from 1100 TCGA L-R breast tumors. DNMTs present significant increased expression on L-sided tumors, as compared to the R ones. This is not accompanied by the TET enzymes (panel B), which do not differ in their expression regarding the side.

Figure 6. L-R Proliferation rate comparison by KI67 and mitotic index. A. Comparison of L-R KI67 expression in 1060 primary breast tumors from TCGA. L expression in significantly increased (Unpaired T-test, p=0.002). B. Proportion of 70 L-R IDC breast tumors from local patients with high and low mitotic count (Fisher exact Test, p=0.002).

647

648 **TABLES**

649 **Table 1. L-R Differential Methylation of Ion Channels in in-vivo and in-silico studies.**

ION CHANNELS FROM IN-VIVO ASSAYS

More Methylated Right		More Methylated Left	
Gene Symbol[a]	**Channel Function**	**Gene Symbol***	**Channel Function**
CHRNE	DEPOLARIZATION	*ASIC2*	DEPOLARIZATION
HTR1A	DEPOLARIZATION	*CACNA1A*	DEPOLARIZATION
PIEZO2	DEPOLARIZATION	*CACNA2D2*	DEPOLARIZATION
RYR3	DEPOLARIZATION	*CATSPERD*	DEPOLARIZATION
TRPC7	DEPOLARIZATION	*PKD1L1*	DEPOLARIZATION
TRPM8	DEPOLARIZATION	*TRPM4*	DEPOLARIZATION
ANO2	HYPERPOLARIZATION	*ANO3*	HYPERPOLARIZATION
ATP1A3	HYPERPOLARIZATION	*ANO5*	HYPERPOLARIZATION
ATP6V1C2	HYPERPOLARIZATION	*CLCN1*	HYPERPOLARIZATION
ATP6V1H	HYPERPOLARIZATION	*CLIC5*	HYPERPOLARIZATION
GABBR1	HYPERPOLARIZATION	*GABBR2*	HYPERPOLARIZATION
KCNA7	HYPERPOLARIZATION	*GABRA5*	HYPERPOLARIZATION
KCNB1	HYPERPOLARIZATION	*GABRD*	HYPERPOLARIZATION
		GABRG1	HYPERPOLARIZATION
		KCNH2	HYPERPOLARIZATION
		KCNIP3	HYPERPOLARIZATION
		KCNJ18	HYPERPOLARIZATION
		KCNK9	HYPERPOLARIZATION
		KCNN1	HYPERPOLARIZATION
		VDAC2	HYPERPOLARIZATION

ION CHANNELS FROM IN-SILICO ASSAYS

More methylated Right		More Methylated Left	
Gene Symbol*	**Channel Function**	**Gene Symbol***	**Channel Function**

CACNA1D	DEPOLARIZATION
CACNA1H	DEPOLARIZATION
CACNA1I	DEPOLARIZATION
CACNB2	DEPOLARIZATION
CACNG4	DEPOLARIZATION
CACNG6	DEPOLARIZATION
CHRNA6	DEPOLARIZATION
CHRNB1	DEPOLARIZATION
CHRNB2	DEPOLARIZATION
CNGA3	DEPOLARIZATION
GRIA1	DEPOLARIZATION
HVCN1	DEPOLARIZATION
LRRC8D	DEPOLARIZATION
LRRC8E	DEPOLARIZATION
MCOLN2	DEPOLARIZATION
MCOLN3	DEPOLARIZATION
PKD2L2	DEPOLARIZATION
SCN3B	DEPOLARIZATION
SCN9A	DEPOLARIZATION
SCNN1G	DEPOLARIZATION
TRPA1	DEPOLARIZATION
TRPC2	DEPOLARIZATION
TRPC3	DEPOLARIZATION
TRPM2	DEPOLARIZATION
TRPM6	DEPOLARIZATION
TRPV3	DEPOLARIZATION
TRPV4	DEPOLARIZATION
TRPV6	DEPOLARIZATION
CLIC3	HYPERPOLARIZATION
GABRA2	HYPERPOLARIZATION
GABRG1	HYPERPOLARIZATION
GABRP	HYPERPOLARIZATION
CACNA2D2	DEPOLARIZATION
CACNA2D4	DEPOLARIZATION
CHRNA1	DEPOLARIZATION
CNGA1	DEPOLARIZATION
P2RX4	DEPOLARIZATION
PKD2	DEPOLARIZATION
RYR1	DEPOLARIZATION
SCN11A	DEPOLARIZATION
SCNN1A	DEPOLARIZATION
TRPM3	DEPOLARIZATION
CFTR	HYPERPOLARIZATION
CLCN1	HYPERPOLARIZATION
CLCNKB	HYPERPOLARIZATION
HCN1	HYPERPOLARIZATION
KCNA1	HYPERPOLARIZATION
KCNA5	HYPERPOLARIZATION
KCNC3	HYPERPOLARIZATION
KCNH7	HYPERPOLARIZATION
KCNH8	HYPERPOLARIZATION
KCNJ9	HYPERPOLARIZATION
KCNMA1	HYPERPOLARIZATION
KCNS2	HYPERPOLARIZATION

GABRR1	HYPERPOLARIZATION
GLRA3	HYPERPOLARIZATION
GLRB	HYPERPOLARIZATION
KCNA2	HYPERPOLARIZATION
KCNA6	HYPERPOLARIZATION
KCNA7	HYPERPOLARIZATION
KCNG1	HYPERPOLARIZATION
KCNH1	HYPERPOLARIZATION
KCNH4	HYPERPOLARIZATION
KCNH6	HYPERPOLARIZATION
KCNJ15	HYPERPOLARIZATION
KCNJ2	HYPERPOLARIZATION
KCNJ5	HYPERPOLARIZATION
KCNJ6	HYPERPOLARIZATION
KCNK3	HYPERPOLARIZATION
KCNK4	HYPERPOLARIZATION
KCNK5	HYPERPOLARIZATION
KCNN4	HYPERPOLARIZATION
KCNQ3	HYPERPOLARIZATION
KCNQ4	HYPERPOLARIZATION
KCNS1	HYPERPOLARIZATION
KCNS3	HYPERPOLARIZATION
KCNT2	HYPERPOLARIZATION

650 * HUGO Gene Nomenclature Committee (HGNC)

651

652 **REFERENCES**

653 1. Monsoro-Burq AH, Levin M. Avian models and the study of invariant asymmetry: How the

654 chicken and the egg taught us to tell right from left. Int J Dev Biol. 2018.

655 2. Vandenberg LN, Levin M. Far from solved: A perspective on what we know about early

mechanisms of left-right asymmetry. Dev Dyn. 2010.

3. Levin M, Klar AJS, Ramsdell AF. Introduction to provocative questions in left–right asymmetry. Philos Trans R Soc B Biol Sci. 2016;371:20150399. doi:10.1098/rstb.2015.0399.

4. Ma K. Embryonic left-right separation mechanism allows confinement of mutation-induced phenotypes to one lateral body half of bilaterians. Am J Med Genet Part A. 2013.

5. Sutherland MJ, Ware SM. Disorders of left-right asymmetry: Heterotaxy and situs inversus. American Journal of Medical Genetics, Part C: Seminars in Medical Genetics. 2009.

6. McDowell G, Rajadurai S, Levin M. From cytoskeletal dynamics to organ asymmetry: A nonlinear, regulative pathway underlies left - Right patterning. Philos Trans R Soc B Biol Sci. 2016.

7. Soofi M, Alpert MA, Barbadora J, Mukerji B, Mukerji V. HUMAN LATERALITY DISORDERS: PATHOGENESIS, CLINICAL MANIFESTATIONS, DIAGNOSIS, AND MANAGEMENT. Am J Med Sci. 2021.

8. Robichaux JP, Hallett RM, Fuseler JW, Hassell JA, Ramsdell AF. Mammary glands exhibit molecular laterality and undergo left-right asymmetric ductal epithelial growth in MMTV-cNeu mice. Oncogene. 2015;34:2003–10. doi:10.1038/onc.2014.149.

9. Yang SY, Cho MS, Kim NK. Difference between right-sided and left-sided colorectal cancers: from embryology to molecular subtype. Expert Review of Anticancer Therapy. 2018.

10. Campoy EM, Laurito SR, Branham MT, Urrutia G, Mathison A, Gago F, et al. Asymmetric cancer hallmarks in breast tumors on different sides of the body. PLoS One. 2016;11.

11. Atiya HI, Dvorkin-Gheva A, Hassell J, Patel S, Parker RL, Hartstone-Rose A, et al. Intraductal adaptation of the 4T1 mouse model of breast cancer reveals effects of the epithelial

678 microenvironment on tumor progression and metastasis. Anticancer Res. 2019.

679 12. Yi T, Zhang Y, Ng DM, Xi Y, Ye M, Cen L, et al. Regulatory Network Analysis of Mutated
680 Genes Based on Multi-Omics Data Reveals the Exclusive Features in Tumor Immune
681 Microenvironment Between Left-Sided and Right-Sided Colon Cancer. Front Oncol. 2021.

682 13. Hanahan D, Weinberg RA. Hallmarks of cancer: The next generation. Cell. 2011;144:646–
683 74.

684 14. Dawson MA. The cancer epigenome: Concepts, challenges, and therapeutic opportunities.
685 Science. 2017.

686 15. Tammen SA, Friso S, Choi SW. Epigenetics: The link between nature and nurture. Molecular
687 Aspects of Medicine. 2013.

688 16. Okugawa Y, Grady WM, Goel A. Epigenetic Alterations in Colorectal Cancer: Emerging
689 Biomarkers. Gastroenterology. 2015.

690 17. d'Errico M, Alwers E, Zhang Y, Edelmann D, Brenner H, Hoffmeister M. Identification of
691 prognostic DNA methylation biomarkers in patients with gastrointestinal adenocarcinomas: A
692 systematic review of epigenome-wide studies. Cancer Treatment Reviews. 2020.

693 18. Singh A, Gupta S, Sachan M. Epigenetic biomarkers in the management of ovarian cancer:
694 Current prospectives. Front Cell Dev Biol. 2019.

695 19. De Almeida BP, Apolónio JD, Binnie A, Castelo-Branco P. Roadmap of DNA methylation in
696 breast cancer identifies novel prognostic biomarkers. BMC Cancer. 2019.

697 20. Marzese DM, Gago FE, Vargas-Roig LM, Roqué M. Simultaneous analysis of the methylation
698 profile of 26 cancer related regions in invasive breast carcinomas by MS-MLPA and drMS-
699 MLPA. Mol Cell Probes. 2010;24.

700 21. Marzese DM, Hoon DSB, Chong KK, Gago FE, Orozco JI, Tello OM, et al. DNA methylation
701 index and methylation profile of invasive ductal breast tumors. J Mol Diagnostics. 2012;14.

702 22. Branham MT, Marzese DM, Laurito SR, Gago FE, Orozco JI, Tello OM, et al. Methylation
703 profile of triple-negative breast carcinomas. Oncogenesis. 2012;1.

704 23. Urrutia G, Laurito S, Marzese DM, Gago F, Orozco J, Tello O, et al. Epigenetic variations in
705 breast cancer progression to lymph node metastasis. ClinExpMetastasis. 2015;32:99–110.

706 24. Marzese DM, Scolyer RA, Roqué M, Vargas-Roig LM, Huynh JL, Wilmott JS, et al. DNA
707 methylation and gene deletion analysis of brain metastases in melanoma patients identifies
708 mutually exclusive molecular alterations. Neuro Oncol. 2014;16.

709 25. Marzese DM, Gago FE, Orozco JI, Tello OM, Roqué M, Vargas-Roig LM. Aberrant DNA
710 methylation of cancer-related genes in giant breast fibroadenoma: A case report. J Med Case
711 Rep. 2011;5.

712 26. Cortés-Mendoza J, Díaz de León-Guerrero S, Pedraza-Alva G, Pérez-Martínez L. Shaping
713 synaptic plasticity: The role of activity-mediated epigenetic regulation on gene transcription.
714 Int J Dev Neurosci. 2013.

715 27. Tseng AS, Levin M. Transducing Bioelectric Signals into Epigenetic Pathways During Tadpole
716 Tail Regeneration. Anatomical Record. 2012.

717 28. Penas C, Navarro X. Epigenetic modifications associated to neuroinflammation and
718 neuropathic pain after neural trauma. Frontiers in Cellular Neuroscience. 2018.

719 29. Levin M, Selberg J, Rolandi M. Endogenous Bioelectrics in Development, Cancer, and
720 Regeneration: Drugs and Bioelectronic Devices as Electroceuticals for Regenerative Medicine.
721 iScience. 2019.

722 30. Levin M. Bioelectric signaling: Reprogrammable circuits underlying embryogenesis,
723 regeneration, and cancer. Cell. 2021.

724 31. Blackiston DJ, McLaughlin KA, Levin M. Bioelectric controls of cell proliferation: Ion
725 channels, membrane voltage and the cell cycle. Cell Cycle. 2009.

726 32. Onjiko RM, Morris SE, Moody SA, Nemes P. Single-cell mass spectrometry with multi-
727 solvent extraction identifies metabolic differences between left and right blastomeres in the 8-
728 cell frog (Xenopus) embryo. Analyst. 2016;141:3648–56. doi:10.1039/C6AN00200E.

729 33. Mittwoch U. Different gene expressions on the left and the right: A genotype/phenotype
730 mismatch in need of attention. Ann Hum Genet. 2008;72:2–9.

731 34. Levin M, Thorlin T, Robinson KR, Nogi T, Mercola M. Asymmetries in H+/K+-ATPase and cell
732 membrane potentials comprise a very early step in left-right patterning. Cell. 2002.

733 35. Pai VP, Vandenberg LN, Blackiston D, Levin M. Neurally derived tissues in xenopus laevis
734 embryos exhibit a consistent bioelectrical left-right asymmetry. Stem Cells Int. 2012.

735 36. Kenney NJ, Adkins HB, Sanicola M. Nodal and cripto-1: Embryonic pattern formation genes
736 involved in mammary gland development and tumorigenesis. Journal of Mammary Gland
737 Biology and Neoplasia. 2004.

738 37. Garfinkel L, CRAIG L, SEIDMAN H. An appraisal of left and right breast cancer. JNatlCancer
739 Inst. 1959;23:617–31.

740 38. Baran B, Mert Ozupek N, Yerli Tetik N, Acar E, Bekcioglu O, Baskin Y. Difference Between
741 Left-Sided and Right-Sided Colorectal Cancer: A Focused Review of Literature. Gastroenterol
742 Res. 2018.

743 39. Sponholz S, Oguzhan S, Mese M, Schirren M, Kirschbaum A, Schirren J. The impact of

744 primary tumor location on prognosis after colorectal lung metastasectomy. Int J Colorectal Dis.
745 2021.

746 40. Ni J, Cui N, Wang Y, Liu J. Case Report: Bilateral Renal Cell Carcinoma With Different
747 Histological and Morphological Features, Clear Cell and Cystic Thyroid-Like Follicular Subtype.
748 Front Oncol. 2021.

749 41. Guo S, Yao K, He X, Wu S, Ye Y, Chen J, et al. Prognostic significance of laterality in renal cell
750 carcinoma: A population-based study from the surveillance, epidemiology, and end results
751 (SEER) database. Cancer Med. 2019.

752 42. Połczyńska MM, Beck L, Kuhn T, Benjamin CF, Ly TK, Japardi K, et al. Tumor location and
753 reduction in functional MRI estimates of language laterality. J Neurosurg. 2021.

754 43. He X, Zhao X, Wang X, Liang G, Qi H, Zhu C, et al. Distinctive pattern of left–right
755 asymmetry of ovarian benign teratomas in Chinese population: a 12-year-long cross-sectional
756 study. Arch Gynecol Obstet. 2021.

757 44. Hussain Z. Impact of laterality on cumulative survival in patients diagnosed with
758 retinoblastoma: A retrospective cohort analysis of 1925 cases in the surveillance,
759 epidemiology, and end results (seer) program. Clin Ophthalmol. 2021.

760 45. Busk T, Clemmesen J. The frequencies of left-and right-sided breast cancer. Br J Cancer.
761 1947.

762 46. Roychoudhuri R, Putcha V, Møller H. Cancer and laterality: A study of the five major paired
763 organs (UK). Cancer Causes Control. 2006.

764 47. Klann E, Williamson JM, Tagliamonte MS, Ukhanova M, Asirvatham JR, Chim H, et al.
765 Microbiota composition in bilateral healthy breast tissue and breast tumors. Cancer Causes
766 Control. 2020.

767 48. Mishra P, Chan DC. Mitochondrial dynamics and inheritance during cell division,
768 development and disease. Nature Reviews Molecular Cell Biology. 2014.

769 49. McLean CY, Bristor D, Hiller M, Clarke SL, Schaar BT, Lowe CB, et al. GREAT improves
770 functional interpretation of cis-regulatory regions. Nat Biotechnol. 2010.

771 50. Emran A Al, Marzese DM, Menon DR, Stark MS, Torrano J, Hammerlindl H, et al. Distinct
772 histone modifications denote early stress-induced drug tolerance in cancer. Oncotarget. 2018.

773 51. Nygren AOH, Ameziane N, Duarte HMB, Vijzelaar RNCP, Waisfisz Q, Hess CJ, et al.
774 Methylation-Specific MLPA (MS-MLPA): Simultaneous detection of CpG methylation and copy
775 number changes of up to 40 sequences. Nucleic Acids Res. 2005.

776 52. Ogston KN, Miller ID, Payne S, Hutcheon AW, Sarkar TK, Smith I, et al. A new histological
777 grading system to assess response of breast cancers to primary chemotherapy: Prognostic
778 significance and survival. Breast. 2003;12:320–7.

779 53. Russell TD, Jindal S, Agunbiade S, Gao D, Troxell M, Borges VF, et al. Myoepithelial cell
780 differentiation markers in ductal carcinoma in situ progression. Am J Pathol. 2015.

781 54. Bates E. Ion Channels in Development and Cancer. Annu Rev Cell Dev Biol. 2015.

782 55. Harris MP. Bioelectric signaling as a unique regulator of development and regeneration.
783 Development (Cambridge). 2021.

784 56. Levin M, Pezzulo G, Finkelstein JM. Endogenous Bioelectric Signaling Networks: Exploiting
785 Voltage Gradients for Control of Growth and Form. Annu Rev Biomed Eng. 2017.

786 57. Bonzanni M, Payne SL, Adelfio M, Kaplan DL, Levin M, Oudin MJ. Defined extracellular ionic
787 solutions to study and manipulate the cellular resting membrane potential. Biol Open. 2020.

788 58. Meadows JP, Guzman-Karlsson MC, Phillips S, Brown JA, Strange SK, Sweatt JD, et al.

789 Dynamic DNA methylation regulates neuronal intrinsic membrane excitability. Sci Signal. 2016.

790 59. Zhou W, Dinh HQ, Ramjan Z, Weisenberger DJ, Nicolet CM, Shen H, et al. DNA methylation
791 loss in late-replicating domains is linked to mitotic cell division. Nat Genet. 2018.

792 60. Inzé D, De Veylder L. Cell cycle regulation in plant development. Annual Review of
793 Genetics. 2006.

794 61. Rosendo-Pineda MJ, Moreno CM, Vaca L. Role of ion channels during cell division. Cell
795 Calcium. 2020.

796 62. Fields C, Bischof J, Levin M. Morphological coordination: A common ancestral function
797 unifying neural and non-neural signaling. Physiology. 2020.

798 63. Martinez-Corral R, Liu J, Prindle A, Süel GM, Garcia-Ojalvo J. Metabolic basis of brain-like
799 electrical signalling in bacterial communities. Philos Trans R Soc B Biol Sci. 2019.

800 64. Pai VP, Aw S, Shomrat T, Lemire JM, Levin M. Transmembrane voltage potential controls
801 embryonic eye patterning in Xenopus laevis. Development. 2012.

802 65. Pai VP, Lemire JM, Paré JF, Lin G, Chen Y, Levin M. Endogenous gradients of resting
803 potential instructively pattern embryonic neural tissue via notch signaling and regulation of
804 proliferation. J Neurosci. 2015.

805 66. Belus MT, Rogers MA, Elzubeir A, Josey M, Rose S, Andreeva V, et al. Kir2.1 is important for
806 efficient BMP signaling in mammalian face development. Dev Biol. 2018.

807 67. Perathoner S, Daane JM, Henrion U, Seebohm G, Higdon CW, Johnson SL, et al. Bioelectric
808 Signaling Regulates Size in Zebrafish Fins. PLoS Genet. 2014.

809 68. Lanni JS, Peal D, Ekstrom L, Chen H, Stanclift C, Bowen ME, et al. Integrated K+ channel and
810 K+Cl- cotransporter functions are required for the coordination of size and proportion during

811 development. Dev Biol. 2019.

812 69. Dahal GR, Rawson J, Gassaway B, Kwok B, Tong Y, Ptácek LJ, et al. An inwardly rectifying K+
813 channel is required for patterning. Dev. 2012.

814 70. Brook Chernet ML. Endogenous Voltage Potentials and the Microenvironment: Bioelectric
815 Signals that Reveal, Induce and Normalize Cancer. J Clin Exp Oncol. 2014.

816 71. Srivastava P, Kane A, Harrison C, Levin M. A Meta-Analysis of Bioelectric Data in Cancer,
817 Embryogenesis, and Regeneration. Bioelectricity. 2020.

818 72. Prevarskaya N, Skryma R, Shuba Y. Ion channels in cancer: Are cancer hallmarks
819 oncochannelopathies? Physiological Reviews. 2018.

820 73. Becchetti A. Ion channels and transporters in cancer. 1. ion channels and cell
821 proliferationin cancer. Am J Physiol - Cell Physiol. 2011.

822 74. Rao VR, Perez-Neut M, Kaja S, Gentile S. Voltage-gated ion channels in cancer cell
823 proliferation. Cancers. 2015.

824 75. Fraser SP, Ozerlat-Gunduz I, Brackenbury WJ, Fitzgerald EM, Campbell TM, Coombes RC, et
825 al. Regulation of voltage-gated sodium channel expression in cancer: Hormones, growth
826 factors and auto-regulation. Philosophical Transactions of the Royal Society B: Biological
827 Sciences. 2014.

828 76. Burr HS, Strong LC, Smith GM. Bio-Electric Correlates of Methylcolanthrene-Induced
829 Tumors in Mice. Yale J Biol Med. 1938.

830 77. Moore D, Walker SI, Levin M. Cancer as a disorder of patterning information:
831 computational and biophysical perspectives on the cancer problem. Converg Sci Phys Oncol.
832 2017.

833 78. Chernet BT, Levin M. Transmembrane voltage potential of somatic cells controls oncogene-
834 mediated tumorigenesis at long-range. Oncotarget. 2014.

835 79. Levin M. The Computational Boundary of a “Self”: Developmental Bioelectricity Drives
836 Multicellularity and Scale-Free Cognition. Front Psychol. 2019.

837